

UVRM: A Scalable 3D Reconstruction Model from Unposed Videos

Shiu-hong Kao^{1,2,†} Xiao Li¹ Jinglu Wang¹ Chi-Keung Tang² Yu-Wing Tai³ Yan Lu¹

¹Microsoft Research Asia ²Hong Kong University of Science and Technology ³Dartmouth College

{skao, cktang}@cse.ust.hk, yu-wing.tai@dartmouth.edu,

{li.xiao, jinglu.wang, yanlu}@microsoft.com

Abstract

Large Reconstruction Models (LRMs) have recently become a popular method for creating 3D foundational models. Training 3D reconstruction models with 2D visual data traditionally requires prior knowledge of camera poses for the training samples, a process that is both time-consuming and prone to errors. Consequently, 3D reconstruction training has been confined to either synthetic 3D datasets or small-scale datasets with annotated poses. In this study, we investigate the feasibility of 3D reconstruction using unposed video data of various objects. We introduce *UVRM*, a novel 3D reconstruction model capable of being trained and evaluated on monocular videos without requiring any information about the pose. *UVRM* uses a transformer network to implicitly aggregate video frames into a pose-invariant latent feature space, which is then decoded into a tri-plane 3D representation. To obviate the need for ground-truth pose annotations during training, *UVRM* employs a combination of the score distillation sampling (SDS) method and an analysis-by-synthesis approach, progressively synthesizing pseudo novel-views using a pre-trained diffusion model. We qualitatively and quantitatively evaluate *UVRM*'s performance on the *G-Objaverse* and *CO3D* datasets without relying on pose information. Extensive experiments show that *UVRM* is capable of effectively and efficiently reconstructing a wide range of 3D objects from unposed videos.

1. Introduction

The task of digitally reproducing, modifying, and photo-realistically rendering 3D scenes and objects stands as a core research area in computer vision, with wide-ranging applications. As digital landscapes and interactive technologies increasingly pervade sectors such as entertainment, robotics, and design, the demand for scalable and adaptable 3D models is at an all-time high. Recent breakthroughs in neural 3D representations, initiated by

[†]Work mainly done during internship at Microsoft Research Asia.

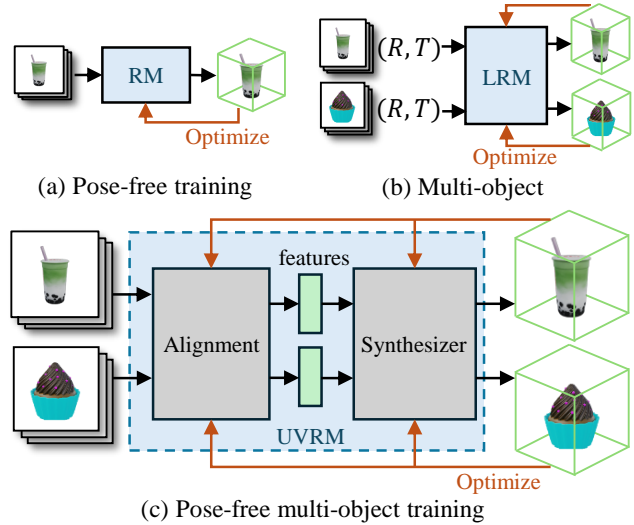


Figure 1. Different from previous methods, which either focus on (a) per-scene pose-free training or (b) 3D reconstruction model trained with known camera poses, we propose *UVRM* (c) aims for a fully pose-free training of 3D reconstruction model from 2D observations.

NeRF [19] and expanded upon by subsequent methods like 3DGS [13] have achieved unprecedented results, paving the way for the creation of generalized 3D foundation models. These models, analogous to the progress in natural language processing and text-to-image models in computer vision, will enable more efficient and flexible 3D content generation, manipulation, and interaction at scale.

Large Reconstruction Models (LRMs) have contributed notable development on 3D foundation models, offering the ability to reconstruct 3D representations from various objects or scenes in a single forward pass. Currently, LRMs are trained on synthetic 3D datasets, like Objaverse [7] and its derivatives. Although effective for now, the reliance on synthetic 3D data is increasingly seen as a bottleneck due to the upper-bound quantity and quality of such data, especially in comparison to the abundant data available in image, video, and speech domains. To overcome this, alter-

native approaches for 3D reconstruction training use large video and image datasets. However, these approaches require precise camera poses to align 3D representations with their corresponding 2D observations for training using reconstruction losses such as render loss. The scarcity of multi-view datasets with accurate pose annotations, combined with the challenges of estimating camera poses from arbitrary images or videos, due to issues like homogeneous regions or view-dependent appearances, poses a significant barrier. Thus, creating a pose-free training and inference framework for 3D reconstruction is crucial for scaling 3D reconstruction efficiently and advancing toward the goal of building generalized 3D foundation models.

In this paper, we take an important step toward harnessing large-scale 2D datasets for 3D reconstruction. Our primary objective is to explore whether it is feasible to train a 3D reconstruction model for various objects, using only monocular videos without any pose annotations. We tackle this inquiry from two angles:

- **Pose-free alignment** - *Is it possible to achieve 3D reconstruction from an arbitrary number of input views without explicit pose alignment?*
- **Pose-free training** - *Can we train a reconstruction model solely with 2D data, devoid of pose annotations?*

We affirmatively answer these questions by introducing UVRM, a **Reconstruction Model for Unposed Videos**. To tackle the first question, we propose encoding 3D scenes using viewpoint-invariant features. This differs from traditional approaches, which typically focus on estimating view-specific or pixel-aligned features with explicit pose calibration. Our method encodes all input views into a unified latent space, utilizing a transformer-based model to implicitly aggregate information from multiple views. The result is a latent feature with viewpoint-invariant tokens. This strategy allows for the scaling of inputs to dense, pose-free multi-view images without compromising on memory or computational efficiency. These viewpoint-invariant tokens can then be decoded into a neural 3D representation suitable for rendering. To address the second question, we integrate the Score Distillation Sampling (SDS) method with an analysis-by-synthesis strategy. This involves incrementally augmenting view-consistent pseudo-views using pre-trained diffusion models throughout the training process. Our method circumvents the need to calculate render loss between input and reconstructed views during training, thereby obviating the necessity for ground truth pose annotations for input videos.

We evaluate our model’s performance on the synthetic G-Objaverse dataset [44] without using of pose information, as well as CO3D [24] dataset with real-world videos. We demonstrate that the proposed UVRM can reconstruct various 3D objects from pose-free monocular videos. Notably, UVRM outperforms prior pose-free NeRF methods

that rely on per-object optimization, showcasing superior results. Our contributions can be summarized as:

- A new research problem of training 3D reconstruction model from 2D datasets without explicit pose calibration.
- A new method that takes pose-free monocular videos as input for 3D object reconstruction.
- A novel training pipeline that eliminates pose annotations for training 3D reconstruction models.

2. Related Work

Neural 3D Representations. The neural field representation of 3D scenes has attracted significant attention from the literature since the pioneer work of NeRF [19]. NeRF has demonstrated its effectiveness on the task of view synthesis from multi-view posed images, leading to a number of follow-up works that extend its capabilities. Some representative works including NeUS [32], Tri-plane [3], and Gaussian splatting [13]. These techniques utilize multi-layer perceptrons to generate implicit or hybrid fields such as sign distance functions or volume radiance fields. Our method leverage the expressiveness of neural representations, aims to reconstruct 3D objects with minimal requirement of inputs (i.e., pose-free monocular video).

Multi-view 3D Reconstruction. Vanilla multi-view reconstruction method, regardless of its 3D representations, requires accurate camera poses. Camera poses are often obtained from Structure-from-Motion (SfM) methods such as COLMAP [28], which significantly increases the time cost and risk of failure, due to the sensitivity of traditional feature matching strategy. Some recent works incorporates this pipeline with neural representations to jointly improve the reconstruction quality and camera estimation robustness [8, 9, 34, 37, 39]. Another stream of works rely on additional information such as depth [2, 29] or optical flow [18]. Our method focus on 3D reconstruction from pose-free videos without explicit pose calibration.

Large Reconstruction Models. Considering the expensive time complexity of per-scene optimization, many works have proposed training a large reconstruction model for multiple objects or scenes. These methods directly reconstruct the 3D representation in a feed-forward pass. Early approaches directly train a CNN-based network to predict neural points [36] or multi-plane images (MPIs) [43], synthesizing novel views via rendering methods such as alpha compositing or point splatting. PixelNeRF [40] predicts pixel-aligned features from images for conditional radiance field. Following works improve the performance of multi-scene model using feature matching [4–6, 35], geometry-aware attention [16, 20], large transformer backbone [11, 33, 41], or 3D volume representations [38]. We do not directly train a LRM in this paper; instead, we focus on developing a new technology for reconstructing 3D objects from pose-free videos, offering novel insights for future ex-

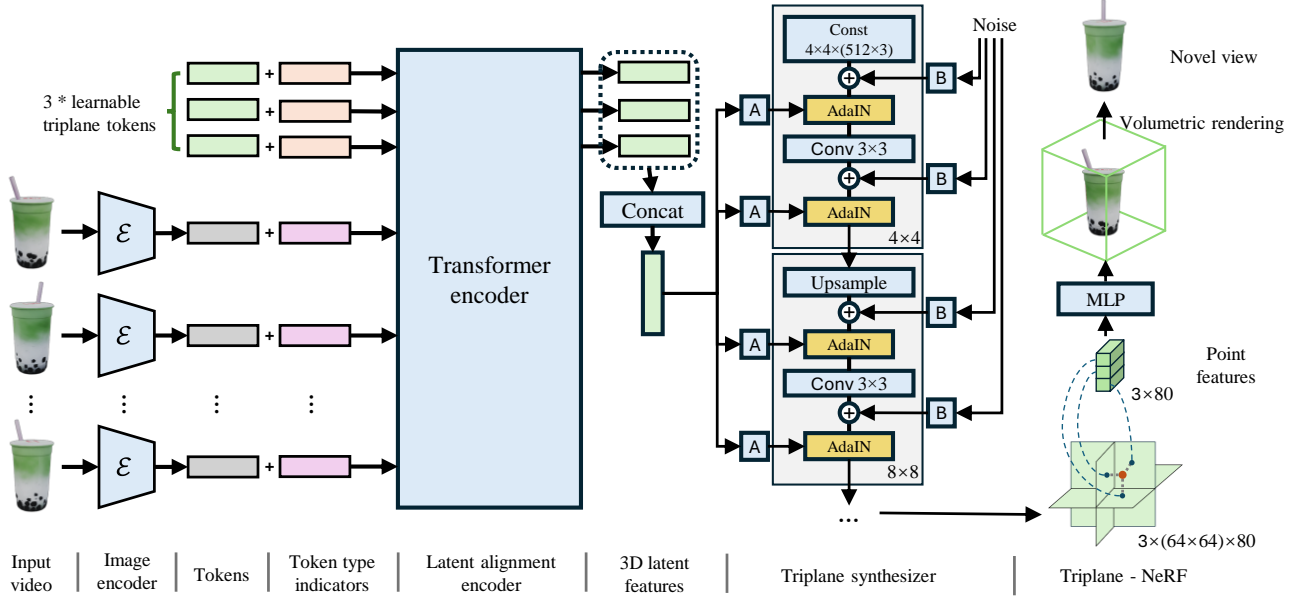


Figure 2. **UVRM architecture.** We propose UVRM, a transformer-based reconstruction model for pose-free monocular video inputs. It first encodes each input view into latent space with a VAE encoder [14]. Next, it adopts a T5-based transformer encoder [22] to extract a pose-invariant feature by implicitly aligning the image latent sequence. The extracted feature are then used modulate a style-based [12] synthesizer to output a tri-plane representation. Here “A” implies a learned affine transform, and “B” stands for learned per-channel scaling factors to the noise input.

pansion of LRM training to large-scale visual datasets.

3. Method

We aim to train a 3D reconstruction model (i.e., the UVRM) from collections of unposed video sequences, each representing one object from different views. Our solution (Fig. 2) consists of two key components: a pose-free, multi-view transformer that implicitly aligns an arbitrary number of RGB frame sequence into a pose-invariant latent feature (Subsection 3.2), and a novel training framework that eliminates the usage of ground-truth poses to compute the render loss for reconstruction (Subsection 3.3). Our framework is build upon the recent advance of neural 3D representations and a diffusion prior with score distillation sampling. We will therefore first introduce some preliminaries in Subsection 3.1. Then, we introduce the pose-free alignment and the pose-free training in following subsections.

3.1. Preliminaries

Triplane NeRF. A Neural Radiance Field (NeRF) is a 5D function that represents the volumetric radiance of any 3D objects [19]. The vanilla NeRF adopts a fully implicit approach, querying the radiance at each position with a MLP network. A triplane is an hybrid NeRF representation for 3D objects [3, 10], which is composed of three axis-aligned feature planes $T = (T_{XY}, T_{XZ}, T_{YZ})$, each with the dimension of $H \times W \times d_T$, where $H \times W$ is the spatial resolution

and d_T is the number of feature channels. Triplane queries the radiance value by first projected 3D positions onto each of the axis-aligned plane and query the corresponding point features $\hat{T} \in \mathbb{R}^{3 \times d_T}$. These features are then decoded into color and density via a smaller MLP. We adopt the tri-plane NeRF as our neural representation for 3D objects.

Score Distillation Sampling (SDS). SDS is a powerful loss function for training 3D generative models from text [21, 30], which can be regarded as a prior that maximizes the agreement of the rendered image from some 3D representations with given text condition. It works by providing gradients towards image formed through the conditional denoising process of a pre-trained diffusion model applied on the rendered image [1]. Formally, given a parametric 3D representation g_Θ and a random camera pose p_r , the SDS loss can be written as:

$$\mathcal{I} = g_\Theta(p_r) \quad (1)$$

$$\mathcal{I}_t = \sqrt{\alpha_t} \mathcal{I} + \sqrt{1 - \alpha_t} \epsilon \quad (2)$$

$$\nabla_{\Theta} \mathcal{L}_{SDS} = \mathbb{E}_{t, p_r, \epsilon} \left[w(t) (\epsilon_\phi(\mathcal{I}_t; t, e) - \epsilon) \frac{\partial \mathcal{I}}{\partial \Theta} \right] \quad (3)$$

where $w(\cdot)$ is a weighting function for denoising timestep t , $\epsilon \sim \mathcal{N}(0, 1)$ is a random Gaussian noise, $\epsilon_\phi(\cdot)$ is the noise predicting function, i.e., the pre-trained diffusion network with parameters ϕ , and e is the given text embedding. We show (in later section) that the SDS loss can be adopted as

a weak-supervised loss for multi-view reconstruction from pose-free video frames.

3.2. UVRM Architecture

Our UVRM model takes an arbitrary numbers of video frames as input and produces a tri-plane that represents the object in the video. It consists of three components: an image encoder, a latent alignment encoder, and a triplane synthesizer.

Image encoder. We utilize the encoder of a pretrained VAE from stable diffusion [25], which projects a given video $\mathcal{V} \in \mathbb{R}^{H \times W \times 3}$ into a latent $\hat{\ell} \in \mathbb{R}^{h \times w \times d}$ with smaller resolution. Each frame in the video is encoded and flattened, forming a token sequence $\ell \in \mathbb{R}^{N \times d'}$ where N is the number of frames in the input video and $d' = h \times w \times d$.

Latent alignment encoder. The pre-processed token sequence ℓ can be of arbitrary length, with each token representing the object in arbitrary and unknown poses. Before reconstructing the 3D representation that is applicable for rendering, we first leverage a transformer model to compress the token sequence into a fixed number of tokens. During the compression training, the transformer model eventually learns to ignore obstructions and focused on implicitly aligns different input tokens of pose-free view observations into these unified, fixed number of tokens, forming a complete latent representation of the 3D object in the video. We implement this process by using three learnable tokens $t \in \mathbb{R}^{3 \times d'}$ representing the 3D latent feature. The information of input tokens are compressed into t using a transformer encoder \mathcal{T} [31], by prefixing the 3D latent t to the video token sequence ℓ as prompts:

$$\hat{t}, \dots = \mathcal{T}(t + t^T, \ell + t^V), \quad (4)$$

where $t^V \in \mathbb{R}^{d'}$ and $t^T \in \mathbb{R}^{d'}$ are token type indicators. We only extracts the first three tokens in the output sequences corresponding to compressed 3D latent and concatenate them as the 3D latent features $\mathbf{F} \in \mathbb{R}^{(3 \times d')}$.

Triplane synthesizer. We use a style-based triplane synthesizer [12] (Fig. 2) to decode the 3D latent features into a triplane. Similar to [12], the triplane synthesizer progressively decodes a set of learnable feature maps into a triplane feature $T \in \mathbb{R}^{3 \times H_T \times W_T \times d_T}$ with stacked convolution layers. The encoded 3d latent token \mathbf{F} modulates each convolution layer output \mathbf{x}_i with an adaptive instance normalization (AdaIN) layer:

$$(\mathbf{y}_{s,i}, \mathbf{y}_{b,i}) = \mathbf{A}_i(\mathbf{F}) \quad (5)$$

$$\text{AdaIN}(\mathbf{x}_i, \mathbf{y}) = \mathbf{y}_{s,i} \frac{\mathbf{x}_i - \mu(\mathbf{x}_i)}{\sigma(\mathbf{x}_i)} + \mathbf{y}_{b,i}, \quad (6)$$

where each \mathbf{A}_i is a learnable affine transformation layer. We then following the volumetric rendering method in [3] to query the radiance field for rendering images.

3.3. Pose-free Training

The UVRM we introduced in Sec. 3.2 has eliminated the requirement of explicit camera calibration for video inputs. However, existing pipelines for 3D reconstruction, still require pose annotations during training. Pose annotations are used to render the 3D representation into reference views w.r.t. the input video for computing reconstruction loss. In contrast, we propose a pose-free training pipeline which combines both **weak supervision** and **self-supervision**. Specifically, we **weakly supervise** the training with the SDS loss, and **self-supervise** the training using pseudo novel views that are generated from the model itself.

Weak-supervision with SDS loss. For multi-view reconstruction, we replacing the condition ϵ of the SDS loss with input video $\mathcal{V}_{gt} = \{\mathcal{I}_{gt}\}$:

$$\nabla_{\Theta} \mathcal{L}_{SDS} = \mathbb{E}_{t, p_r, \epsilon} \left[w(t) (\epsilon_{\phi}(\mathcal{I}_t(p_r, \Theta); t, \mathcal{I}(p_{gt})) - \epsilon) \frac{\partial \mathcal{I}}{\partial \Theta} \right] \quad (7)$$

where ϵ_{ϕ} is the noise prediction network p_r is random sample camera pose for rendering, and p_{gt} is the ground truth pose (unknown for us) of input image \mathcal{I}_{gt} .

A good property of Eq. (7) is that it attempts to match the distribution of images generated from 3D representations $P(\mathcal{I}|\Theta, p_r)$ to the distribution of ground truth images $P(\mathcal{I}|p_{gt})$, up to an global affine transformation of the camera system (i.e., the matched distribution preserves the relative camera pose between different views). Consequentially, we do not need to access the ground truth pose p_{gt} for computing the loss function.

In practice, we compute Eq. (7) stochastically with a pre-trained image-to-3d diffusion model [17]. In each training step, we randomly render a small number of k views $\{\mathcal{I}_i^S\}$ to estimate the gradient of SDS loss w.r.t a reference image \mathcal{I}^R from the video. The random pose p for $\{\mathcal{I}_i^S\}$ for rendering is sampled as follows:

$$\left\{ p_i = \left(r, \frac{2\pi}{i}, \delta \right) \right\}_{i=1}^k \leftarrow P(k; r, \theta), \quad (8)$$

where $\delta \sim U(-\theta, \theta)$, and k, r, θ are all hyper-parameters with $k \in \mathbb{N}$, $r > 0$, $\theta \in [0, \pi/2]$. This generator samples s camera poses orbiting the center of coordinate system with radius r , fixed azimuth angles, and random polar angles.

One issue of the SDS loss (Eq. (7)) is that a perfect match is only theoretically guaranteed when the randomly sampled pose distribution p_r for rendering the 3D representation matches the unknown, ground truth camera distribution p_{gt} in the video, which is hardly the case when handling real-world videos. The stochastic approximation of the SDS loss also introduces additional uncertainty for the optimization process. Hence, we can only regard the SDS

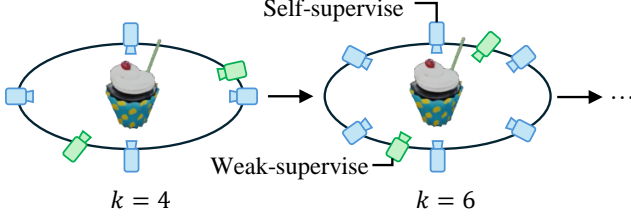


Figure 3. Illustration of our pose-free training framework, where k pseudo-views are randomly synthesized at scattered poses along a given trajectory to achieve self-supervision and SDS regularization at random poses for weak supervision. We iteratively augment more pseudo-views throughout the training process.

loss as a weak supervision for reconstructing a rough 3D representation. In the next section we exploit to further improve the training process by combining additional pixel-wise loss with self-supervision.

Self-supervision by pseudo-view augmentation. A naive approach for self-training is to render additional novel views from the UVRM itself. However, this approach has very limited benefit, as it operates on the UVRM network trained with SDS loss which only forms an approximation of the desired oracle. Our key observation is that re-rendered images of training videos from UVRM (trained with SDS loss) is being optimized towards a specific trajectory, such that each gradient descent step matches a single step of the reversed (i.e., a denoising step) diffusion process. In simple terms, rendered images from UVRM during the intermediate training stage, can be regarded as a set of partially generated images from the denoising process of the pre-trained diffusion model. Hence, we conduct an “analysis-by-synthesis” approach, by simply reusing the same diffusion model to “take over” rendered image from the partially converged UVRM and perform additional denoising steps to augment these images as new pseudo view for further training.

Formally, given the partially converged UVRM model $g(\Theta)$, we first render k images from random views sampled from Eq. (8):

$$\{\mathcal{I}^A\} = \{(g_{\Theta}(p'_i; V), p'_i)\}_{i=1}^{k'} \quad (9)$$

We then add noise perturbation to $\{\mathcal{I}^A\}$ following the forward diffusion process, and using the same diffusion model D in Eq. (3) to synthesis augmented images $\{\mathcal{I}^A\}'$:

$$\mathcal{I}_{i,t}^A = \sqrt{\alpha_{i,t}} \mathcal{I}_{i,t}^A + \sqrt{1 - \alpha_{i,t}} \epsilon \quad (10)$$

$$(\mathcal{I}_i^A)' = D_{\phi}(\mathcal{I}_{i,t}^A, t, \mathcal{I}^R). \quad (11)$$

Finally, we use a combination of the mean square error (MSE) loss and the perceptual loss (LPIPS [42]) in addition to the SDS loss (λ and β are loss weights):

$$\begin{aligned} \mathcal{L}_{\text{recon}} = & \frac{1}{k} \sum_{i=1}^k \text{MSE}(g_{\Theta}(p'_i; V), \mathcal{I}_i^A) \\ & + \lambda \cdot \frac{1}{k} \sum_{i=1}^k \text{LPIPS}(g_{\Theta}(p'_i; V), \mathcal{I}_i^A) \\ & + \frac{1}{\beta} \mathcal{L}_{\text{SDS}}. \end{aligned} \quad (12)$$

Iterative synthesis. The rendered image from UVRM in the early stage is optimized with less steps, referring to early steps in the reversed diffusion process. As the optimization process progresses, the rendered images increasingly resemble the latter stages of the diffusion model’s denoising process, requiring fewer additional denoising steps and less noise intensity. To align with this training process, we introduce an iterative, progressive enhancement strategy that starts with stronger noise $\alpha_{i,t}$, more denoising steps, fewer number of views k , and larger weight (lower β) for the SDS loss in the early stages of training. During the training stage, we iteratively synthesize new pseudo-views with a fixed interval of training steps, gradually reducing the noise intensity, the number of denoising steps, while decreasing the weight for the SDS loss and augmenting more pseudo views. Note that our synthesis at the very beginning of the training stage degrades into purely conditional image generation, which corresponds to the reversed denoising process when $t \rightarrow +\infty$.

Discussion. A straightforward idea for pose-free training is to estimate camera poses for all subjects. We show in later section that indeed UVRM trained with camera poses converges faster and achieves higher quality. Yet this paper aims to propose an orthogonal, new training method different from SfM-based approaches [27], by learning from the camera trajectory distribution to produce 3D pose-invariant latent features, akin to and inspired by human’s mental 3D reconstruction ability without explicit parameter estimation. This idea supports scaling up to larger real-world datasets and bypasses their recurrent problems (e.g., per-scene pose-free training, need dense views, front view only, close poses) in explicit camera estimation. To this end, the weak-supervised SDS loss and the self-supervised augmentation, which are complementary to each other, work best when employed together in our pose-free training pipeline (shown in ablation study). The diffusion-based augmentation cannot synthesize consistent pseudo-views for training without the SDS loss to drive the partially rendered sample towards the denoising trajectory, while the SDS loss itself cannot fully guide the training converged to a high-fidelity solution with sufficient details. Our method works by adapting both supervisions such that their complementary effect is maximized during the whole training stage.

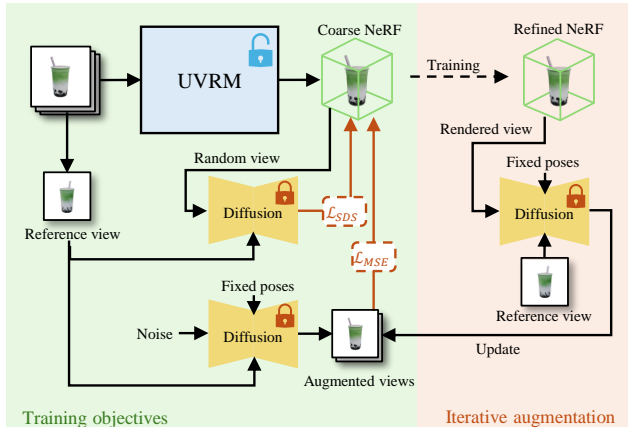


Figure 4. **Iterative augmentation pipeline.** We iteratively alternate between (left, green) weakly supervise training of the UVRM model with score distillation sampling (SDS) on the current set of reference view frames, and (right, orange) generating new set of novel pseudo-views for self-supervised training using the current UVRM and the pre-trained diffusion model. The generated pseudo-views can be trained with pixel-wise render loss.

3.4. Model Training

Model architecture. We use the pretrained VAE from Stable Diffusion 2.1 [26] as our image encoder. The latent alignment encoder is a T5 [23] model with 16 layers with 8 heads and feedforward dimension of 2048. The triplane synthesizer is a StyleGan [12] architecture starting from $4 \times 4 \times 1536$ resolution to $64 \times 64 \times 80$ for each triplane. we use a 4-layer MLP to predict the color and density from triplane features.

Hyper-parameters. We use the Adam [15] optimizer, a learning rate of $1e^{-4}$ with 10k warm-up steps and cosine annealing strategy, and a batch size of 4. λ is set to 1. We linearly increase β from 1 to 25000. We sample 4 random views with $\theta = \frac{\pi}{18}$ to compute SDS in each training step. We perform iterative augmentation every 6000 steps with θ set to 0. k is set 6 at the beginning and increases by 5 for each augmentation iteration.

4. Experiments

To validate our proposed UVRM, we perform an ablation study to demonstrate the ability of our pose-free alignment, the impact of the weak-supervised SDS loss and the self-supervised augmentation strategy. In addition, we perform comparison against two type of existing pose-free methods: an optimization based method for single object and a single image to 3D method. Finally, we show that our solution works well on real-world video sequences.

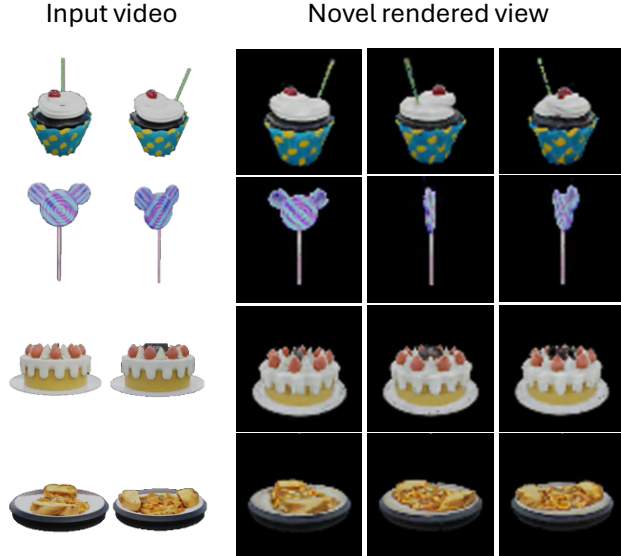


Figure 5. **Capability of pose-free alignment.** UVRM is able to conduct pose-free alignment and 3D reconstruction from a set of monocular videos, which shows great potentials in scalability.

Table 1. **Quantitative comparison.** We compare the full UVRM method to Zero123-XL and variations of UVRM without our designed components.

Model	PSNR(\uparrow)	SSIM(\uparrow)	LPIPS(\downarrow)
Zero123-XL [17]	14.49	0.53	0.23
UVRM (w/o weak-supervise)	15.75	0.69	0.32
UVRM (w/o iterative augmentation)	16.25	0.75	0.24
UVRM (full model)	16.54	0.78	0.22

4.1. Experiment Setup

Dataset. We use the G-Objaverse Food dataset [44] in our ablation study and comparisons. G-Objaverse is a manually annotated subset of the synthetic Objaverse dataset [7] of ten categories, in which the food category consists of 5314 objects. Each sample has a video sequence of 40 views with their associated ground-truth pose; We only use the poses for evaluation and discard them during training. Our real data experiments are conducted on the CO3D Hydrant dataset [24].

Baselines. We compare with two pose-free 3D reconstruction methods that most related to ours: a state-of-the-art, optimization based pose-free NeRF method for single object, Nope-NeRF [2], and a generative image to 3D method (which also serves as our diffusion model used for the SDS loss and view augmentation), Zero123[17]. For baseline methods, we follow their default hyper-parameters and training settings from their official implementation.

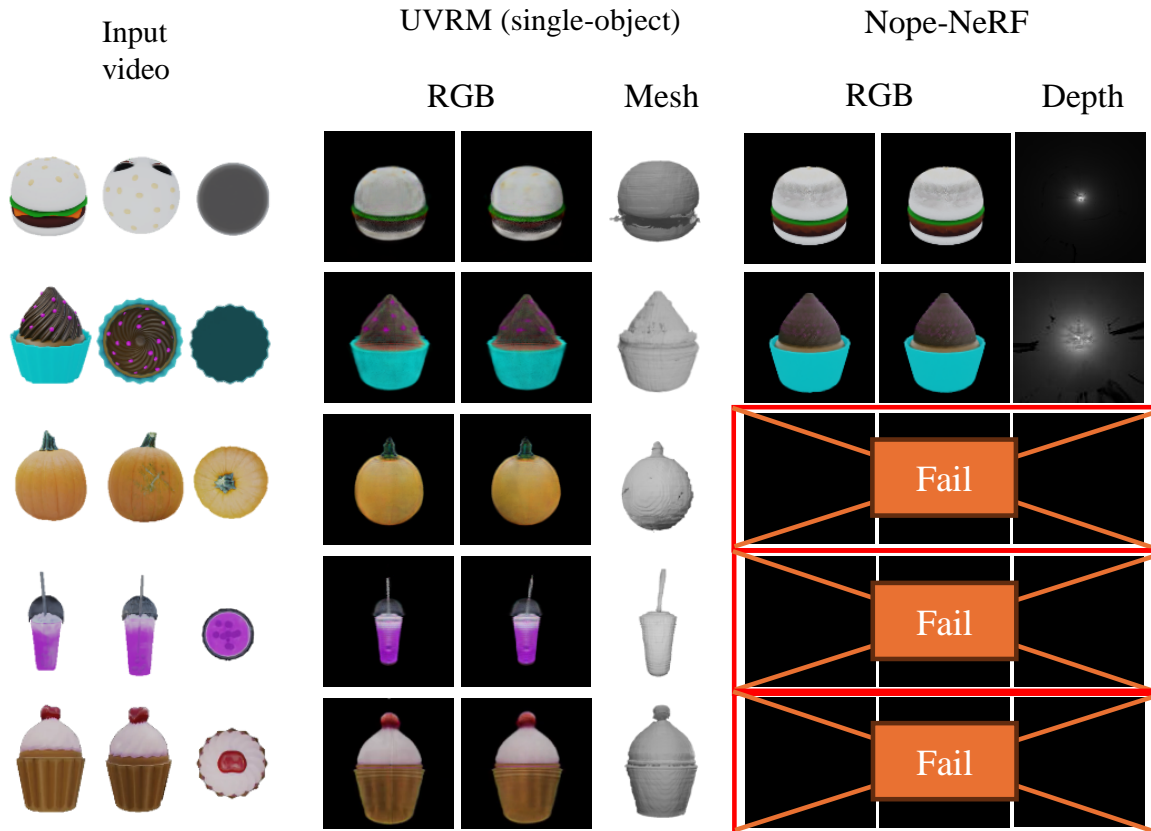


Figure 6. **Comparison of pose-free training on single object.** We compare UVRM with Nope-NeRF [2], the state of the art for NeRF reconstruction with unknown camera poses. In general, UVRM supports more stable reconstruction for 360-degree and sparse views, while Nope-NeRF is shown prone to failure due to the limitation of front view inputs. Depth maps reconstructed from Nope-NeRF also demonstrates a poor reconstructed geometry than ours, while we can directly extract mesh from our UVRM.

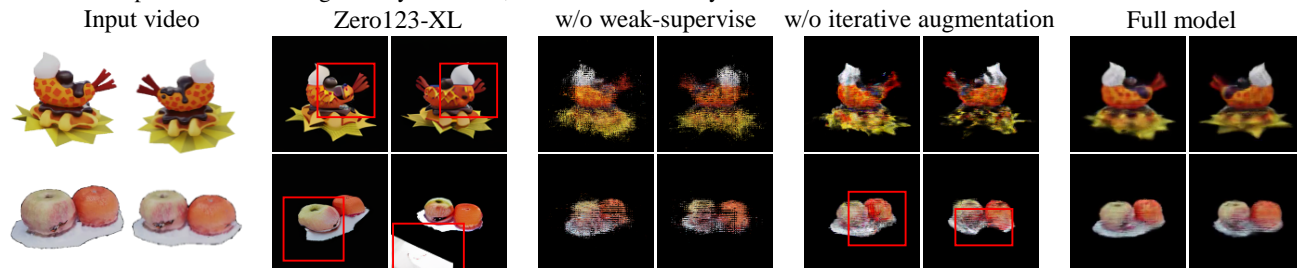


Figure 7. **Ablation study.** Comparison between the full UVRM, the UVRM without certain components, and Zero123-XL [17]. Specifically, Zero123-XL synthesizes high-frequency image but lacks view consistency.

4.2. Ablation Study

Pose-free Alignment. We first validate the capability of the pose-free input alignment of UVRM by training the model on 20 objects randomly sampled from the G-Objaverse Food dataset with known camera poses. To focused on validate the pose-free alignment part without interference, we discard the SDS loss and iterative augmentation and directly use the render MSE loss and LPIPS loss for training. The reconstructed results are demonstrated in Fig. 5. Overall, the UVRM is able to reconstruct various detailed 3D ob-

Table 2. **Runtime Comparison.** We evaluate the reconstruction time cost with 40 input views on A100 GPU. UVRM significantly speed up the per-object reconstruction time, compared to state-of-the-art pose-free training method.

Model	# objects	# GPUs	Total time (hr.)	Avg. (min/obj.)
Nope-NeRF [2]	1	1	6.33	380
UVRM (ours)	1	1	16.5	990
UVRM (ours)	20	4	20.65	62

jects without pose alignment of input views.

Pose-free Training. We train on the same set of 20 objects

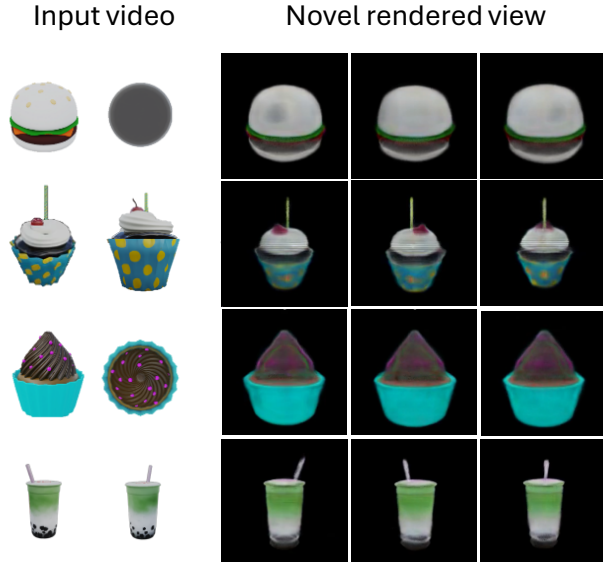


Figure 8. **Results of UVRM with pose-free training on video collections from the G-Objaverse dataset.** The first three rows contains subjects that are also in previous experiments (Figure 5 and 6). Overall, UVRM predicts accurate geometry and texture.

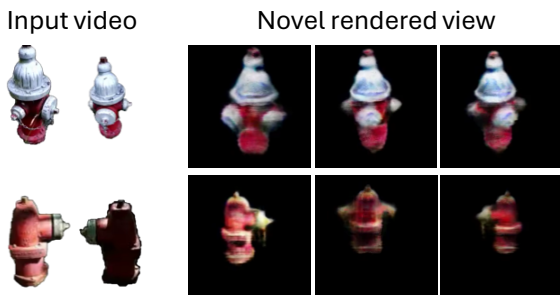


Figure 9. **Multi-object results on real-world data, i.e. CO3D Hydrant [24].** We show that UVRM can not only be trained on multiple objects, but it can also tackle complex objects with non-symmetry and varying shadow.

but this time using our proposed pose-free training pipeline in Sec. 3. As shown in Figure 8, UVRM produces promising results with affordable training complexity (Tab. 2). The first three rows provides comparison with those in Fig. 5 and 6. The last row showcases a more complicated example with highly non-symmetric geometry, where UVRM also produces reasonable results.

Finally, we show that the weak supervision and self-supervision used in our pose-free training pipeline is complementary with equally importance. In Fig. 7 and in Tab. 1, results without the self-supervised augmentation maintains the overall 3D structure but struggling to reconstruct further details. Results without the SDS loss, on the other hand, lose the 3D consistency between different views.

4.3. Comparison

Comparison with pose-free NeRF method. We compare our proposed method with Nope-NeRF [2], the state of the art for pose-free NeRF on single object. For fair comparison, we also train UVRM on single object for 50k steps with the iterative training method. We observe that Nope-NeRF is fragile and fails in many cases (3rd. row to 5th. row in Fig. 6), possibly due to its requirement for dense front views. Our method is robust under all test cases. For objects that both UVRM and Nope-NeRF succeeded (1st and 2nd row in Fig. 6), UVRM reconstructs more accurate 3D geometry and textures than Nope-NeRF. We also compare reconstruction times in Tab. 2. Although our method takes longer to fit a single object compared to Nope-NeRF, its robustness and scalability enable the simultaneous reconstruction of multiple objects, significantly reducing the average time required.

Comparison with single image-to-3D methods. We also compare our method to the single image-to-3D methods Zero123 [17] in Fig. 7 and Tab. 1. While Zero123-XL synthesizes images with high frequency details, it suffers from serious view inconsistency between different views. On the other hand, our UVRMs with weak-supervise training produce more consistent 3D results.

4.4. Results on Real Videos

We demonstrate our method’s ability to perform 3D reconstruction from collections of real-world sequences without camera pose available, on the CO3D Hydrant dataset. Real-world videos in the CO3D dataset exhibits larger pose, shape and appearance variations than synthetic data; nevertheless, UVRM reconstructs reasonable results as shown in Fig. 9. See more results in our supplemental material.

5. Conclusion

We have proposed a new method, UVRM, for 3D object reconstruction from monocular video collections. UVRM is a reconstruction pipeline that is fully pose-free: it utilizes a transformer based structure to implicitly align input video frames with arbitrary camera pose, and a novel training method that simultaneously adopts the score distillation sampling method as a weak supervision and an analysis-by-synthesis approach to iteratively augment pseudo-views as self supervision. We validate our method on both synthetic and real-world datasets without pose information. Our method takes an important step toward using large-scale 2D datasets for 3D reconstruction.

Limitations. While our proof-of-concept experiments have demonstrated the possibility of training 3D reconstruction with pose-free 2D data, we have not generalize our method to a large reconstruction model yet, due to limited time budgets and computational resources.

References

- [1] Thiemo Alldieck, Nikos Kolotouros, and Cristian Sminchisescu. Score distillation sampling with learned manifold corrective. *arXiv preprint arXiv:2401.05293*, 2024. [3](#)
- [2] Wenjing Bian, Zirui Wang, Kejie Li, Jia-Wang Bian, and Victor Adrian Prisacariu. Nope-nerf: Optimising neural radiance field with no pose prior. In *Proceedings of the IEEE/CVF Conference on Computer Vision and Pattern Recognition*, pages 4160–4169, 2023. [2](#), [6](#), [7](#), [8](#), [11](#)
- [3] Eric R Chan, Connor Z Lin, Matthew A Chan, Koki Nagano, Boxiao Pan, Shalini De Mello, Orazio Gallo, Leonidas J Guibas, Jonathan Tremblay, Sameh Khamis, et al. Efficient geometry-aware 3d generative adversarial networks. In *Proceedings of the IEEE/CVF conference on computer vision and pattern recognition*, pages 16123–16133, 2022. [2](#), [3](#), [4](#)
- [4] David Charatan, Sizhe Li, Andrea Tagliasacchi, and Vincent Sitzmann. pixelsplat: 3d gaussian splats from image pairs for scalable generalizable 3d reconstruction. In *arXiv*, 2023. [2](#)
- [5] Yuedong Chen, Haofei Xu, Qianyi Wu, Chuanxia Zheng, Tat-Jen Cham, and Jianfei Cai. Explicit correspondence matching for generalizable neural radiance fields. *arXiv preprint arXiv:2304.12294*, 2023.
- [6] Yuedong Chen, Haofei Xu, Chuanxia Zheng, Bohan Zhuang, Marc Pollefeys, Andreas Geiger, Tat-Jen Cham, and Jianfei Cai. Mvsplat: Efficient 3d gaussian splatting from sparse multi-view images. *arXiv preprint arXiv:2403.14627*, 2024. [2](#)
- [7] Matt Deitke, Dustin Schwenk, Jordi Salvador, Luca Weihs, Oscar Michel, Eli VanderBilt, Ludwig Schmidt, Kiana Ehsani, Aniruddha Kembhavi, and Ali Farhadi. Objaverse: A universe of annotated 3d objects. *arXiv preprint arXiv:2212.08051*, 2022. [1](#), [6](#)
- [8] Zhiwen Fan, Wenyan Cong, Kairun Wen, Kevin Wang, Jian Zhang, Xinghao Ding, Danfei Xu, Boris Ivanovic, Marco Pavone, Georgios Pavlakos, Zhangyang Wang, and Yue Wang. Instantsplat: Unbounded sparse-view pose-free gaussian splatting in 40 seconds, 2024. [2](#)
- [9] Yang Fu, Sifei Liu, Amey Kulkarni, Jan Kautz, Alexei A. Efros, and Xiaolong Wang. Colmap-free 3d gaussian splatting. *arXiv preprint arXiv:2312.07504*, 2023. [2](#)
- [10] Jun Gao, Tianchang Shen, Zian Wang, Wenzheng Chen, Kangxue Yin, Daiqing Li, Or Litany, Zan Gojcic, and Sanja Fidler. Get3d: A generative model of high quality 3d textured shapes learned from images. *Advances In Neural Information Processing Systems*, 35:31841–31854, 2022. [3](#)
- [11] Yicong Hong, Kai Zhang, Jiuxiang Gu, Sai Bi, Yang Zhou, Difan Liu, Feng Liu, Kalyan Sunkavalli, Trung Bui, and Hao Tan. Lrm: Large reconstruction model for single image to 3d. *arXiv preprint arXiv:2311.04400*, 2023. [2](#)
- [12] Tero Karras, Samuli Laine, and Timo Aila. A style-based generator architecture for generative adversarial networks. In *Proceedings of the IEEE/CVF conference on computer vision and pattern recognition*, pages 4401–4410, 2019. [3](#), [4](#), [6](#)
- [13] Bernhard Kerbl, Georgios Kopanas, Thomas Leimkühler, and George Drettakis. 3d gaussian splatting for real-time radiance field rendering. *ACM Trans. Graph.*, 42(4):139–1, 2023. [1](#), [2](#)
- [14] Diederik P Kingma. Auto-encoding variational bayes. *arXiv preprint arXiv:1312.6114*, 2013. [3](#)
- [15] Diederik P Kingma. Adam: A method for stochastic optimization. *arXiv preprint arXiv:1412.6980*, 2014. [6](#)
- [16] Mengfei Li, Xiaoxiao Long, Yixun Liang, Weiyu Li, Yuan Liu, Peng Li, Xiaowei Chi, Xingqun Qi, Wei Xue, Wenhan Luo, et al. M-lrm: Multi-view large reconstruction model. *arXiv preprint arXiv:2406.07648*, 2024. [2](#)
- [17] Ruoshi Liu, Rundi Wu, Basile Van Hoorick, Pavel Tokmakov, Sergey Zakharov, and Carl Vondrick. Zero-1-to-3: Zero-shot one image to 3d object, 2023. [4](#), [6](#), [7](#), [8](#), [11](#)
- [18] Andreas Meuleman, Yu-Lun Liu, Chen Gao, Jia-Bin Huang, Changil Kim, Min H Kim, and Johannes Kopf. Progressively optimized local radiance fields for robust view synthesis. In *Proceedings of the IEEE/CVF Conference on Computer Vision and Pattern Recognition*, pages 16539–16548, 2023. [2](#)
- [19] Ben Mildenhall, Pratul P Srinivasan, Matthew Tancik, Jonathan T Barron, Ravi Ramamoorthi, and Ren Ng. Nerf: Representing scenes as neural radiance fields for view synthesis. *Communications of the ACM*, 65(1):99–106, 2021. [1](#), [2](#), [3](#)
- [20] Takeru Miyato, Bernhard Jaeger, Max Welling, and Andreas Geiger. Gta: A geometry-aware attention mechanism for multi-view transformers. *arXiv preprint arXiv:2310.10375*, 2023. [2](#)
- [21] Ben Poole, Ajay Jain, Jonathan T Barron, and Ben Mildenhall. Dreamfusion: Text-to-3d using 2d diffusion. *arXiv preprint arXiv:2209.14988*, 2022. [3](#)
- [22] Colin Raffel, Noam Shazeer, Adam Roberts, Katherine Lee, Sharan Narang, Michael Matena, Yanqi Zhou, Wei Li, and Peter J. Liu. Exploring the limits of transfer learning with a unified text-to-text transformer. *Journal of Machine Learning Research*, 21(140):1–67, 2020. [3](#)
- [23] Colin Raffel, Noam Shazeer, Adam Roberts, Katherine Lee, Sharan Narang, Michael Matena, Yanqi Zhou, Wei Li, and Peter J Liu. Exploring the limits of transfer learning with a unified text-to-text transformer. *Journal of machine learning research*, 21(140):1–67, 2020. [6](#)
- [24] Jeremy Reizenstein, Roman Shapovalov, Philipp Henzler, Luca Sbordone, Patrick Labatut, and David Novotny. Common objects in 3d: Large-scale learning and evaluation of real-life 3d category reconstruction. In *International Conference on Computer Vision*, 2021. [2](#), [6](#), [8](#)
- [25] Robin Rombach, Andreas Blattmann, Dominik Lorenz, Patrick Esser, and Björn Ommer. High-resolution image synthesis with latent diffusion models, 2021. [4](#)
- [26] Robin Rombach, Andreas Blattmann, Dominik Lorenz, Patrick Esser, and Björn Ommer. High-resolution image synthesis with latent diffusion models. In *Proceedings of the IEEE/CVF Conference on Computer Vision and Pattern Recognition (CVPR)*, pages 10684–10695, 2022. [6](#)
- [27] Johannes Lutz Schönberger and Jan-Michael Frahm. Structure-from-motion revisited. In *Conference on Computer Vision and Pattern Recognition (CVPR)*, 2016. [5](#)

- [28] Johannes L Schonberger and Jan-Michael Frahm. Structure-from-motion revisited. In *Proceedings of the IEEE conference on computer vision and pattern recognition*, pages 4104–4113, 2016. 2
- [29] Wei Sun, Xiaosong Zhang, Fang Wan, Yanzhao Zhou, Yuan Li, Qixiang Ye, and Jianbin Jiao. Correspondence-guided sfm-free 3d gaussian splatting for nvs. *arXiv preprint arXiv:2408.08723*, 2024. 2
- [30] Jiaxiang Tang, Jiawei Ren, Hang Zhou, Ziwei Liu, and Gang Zeng. Dreamgaussian: Generative gaussian splatting for efficient 3d content creation. *arXiv preprint arXiv:2309.16653*, 2023. 3
- [31] A Vaswani. Attention is all you need. *Advances in Neural Information Processing Systems*, 2017. 4
- [32] Peng Wang, Lingjie Liu, Yuan Liu, Christian Theobalt, Taku Komura, and Wenping Wang. NeuS: Learning neural implicit surfaces by volume rendering for multi-view reconstruction. In *NeurIPS*, 2021. 2
- [33] Peng Wang, Hao Tan, Sai Bi, Yinghao Xu, Fujun Luan, Kalyan Sunkavalli, Wenping Wang, Zexiang Xu, and Kai Zhang. Pf-lrm: Pose-free large reconstruction model for joint pose and shape prediction. *arXiv preprint arXiv:2311.12024*, 2023. 2
- [34] Zirui Wang, Shangzhe Wu, Weidi Xie, Min Chen, and Victor Adrian Prisacariu. Nerf-: Neural radiance fields without known camera parameters. *arXiv preprint arXiv:2102.07064*, 2021. 2
- [35] Christopher Wewer, Kevin Raj, Eddy Ilg, Bernt Schiele, and Jan Eric Lenssen. latentsplat: Autoencoding variational gaussians for fast generalizable 3d reconstruction. In *arXiv*, 2024. 2
- [36] Olivia Wiles, Georgia Gkioxari, Richard Szeliski, and Justin Johnson. Synsin: End-to-end view synthesis from a single image. In *Proceedings of the IEEE/CVF conference on computer vision and pattern recognition*, pages 7467–7477, 2020. 2
- [37] Yitong Xia, Hao Tang, Radu Timofte, and Luc Van Gool. Sinerf: Sinusoidal neural radiance fields for joint pose estimation and scene reconstruction. *arXiv preprint arXiv:2210.04553*, 2022. 2
- [38] Haofei Xu, Anpei Chen, Yuedong Chen, Christos Sakaridis, Yulun Zhang, Marc Pollefeys, Andreas Geiger, and Fisher Yu. Murf: Multi-baseline radiance fields. In *Proceedings of the IEEE/CVF Conference on Computer Vision and Pattern Recognition*, pages 20041–20050, 2024. 2
- [39] Lin Yen-Chen, Pete Florence, Jonathan T. Barron, Alberto Rodriguez, Phillip Isola, and Tsung-Yi Lin. inerf: Inverting neural radiance fields for pose estimation. In *2021 IEEE/RSJ International Conference on Intelligent Robots and Systems (IROS)*, pages 1323–1330, 2021. 2
- [40] Alex Yu, Vickie Ye, Matthew Tancik, and Angjoo Kanazawa. pixelnerf: Neural radiance fields from one or few images. In *Proceedings of the IEEE/CVF conference on computer vision and pattern recognition*, pages 4578–4587, 2021. 2
- [41] Kai Zhang, Sai Bi, Hao Tan, Yuanbo Xiangli, Nanxuan Zhao, Kalyan Sunkavalli, and Zexiang Xu. Gs-lrm: Large reconstruction model for 3d gaussian splatting. *arXiv preprint arXiv:2404.19702*, 2024. 2
- [42] Richard Zhang, Phillip Isola, Alexei A Efros, Eli Shechtman, and Oliver Wang. The unreasonable effectiveness of deep features as a perceptual metric. In *Proceedings of the IEEE conference on computer vision and pattern recognition*, pages 586–595, 2018. 5
- [43] Tinghui Zhou, Richard Tucker, John Flynn, Graham Fyffe, and Noah Snavely. Stereo magnification: Learning view synthesis using multiplane images. *arXiv preprint arXiv:1805.09817*, 2018. 2
- [44] Qi Zuo, Xiaodong Gu, Yuan Dong, Zhengyi Zhao, Weihao Yuan, Lingteng Qiu, Liefeng Bo, and Zilong Dong. High-fidelity 3d textured shapes generation by sparse encoding and adversarial decoding. In *European Conference on Computer Vision*, 2024. 2, 6

Appendix

This appendix contains additional implementation details for our training and evaluation as well as more results and ablations.

A. Implementation Details.

Frame Resolutions. In our experiments, all input images are resized to a resolution of 256×256 . The VAE encoder within the UVRM framework encodes each input frame into a feature of dimension $32 \times 32 \times 4$. Additionally, the rendering of the tri-plane and the corresponding back-propagation process are performed at a reduced resolution of 64×64 .

Denoising Timestep Scheduler. In the iterative augmentation process, the denoising timestep scheduler is responsible for determining the amount of noise to be added to the rendered image and the number of denoising steps to be performed. As rendered images are progressively optimized through the denoising process, the desired denoising timestep t , is dependent on the number of training steps s . The scheduler for the denoising timestep during the iterative augmentation process is defined as follows:

$$t \leftarrow \max\left(1 - \frac{s_{curr}}{s_{total}}, 0.2\right) \cdot t_{max}. \quad (\text{A1})$$

Here, t_{max} represents the maximum number of denoising steps, while s_{curr} and s_{total} denote the current training step and the maximum training step, respectively. This approach allows for a gradual reduction in the number of denoising timesteps, with a pre-defined minimal threshold.

Alignment of the Coordinate Systems. To evaluate the quantitative performance of UVRM relative to other methods, we align the reference image, \mathcal{I}^R , with a predefined camera pose, p_0 , and utilize the relative pose between the target and reference views for computation.

B. Additional Results

B.1. Quantitative Comparison

The quantitative comparison results with Nope-NeRF are presented in Tab. A1. Through experimentation, we observed that Nope-NeRF exhibits fragility to certain inputs, occasionally failing to reconstruct any reasonable shape. Consequently, we also include the success rate for Nope-NeRF. In comparison, our method demonstrates greater robustness and achieves superior reconstruction quality.

Table A1. **Reconstruction quality.** Compared with Nope-NeRF, our UVRM achieves higher reconstruction quality and is less fallible for 360-degree video input.

Model	PSNR (\uparrow)	SSIM (\uparrow)	Success rate
Nope-NeRF [2]	12.33	0.71	22%
UVRM	22.43	0.84	100%

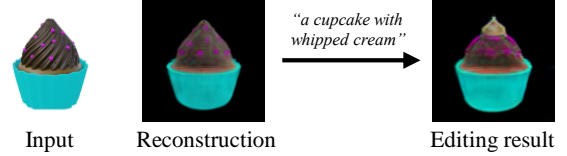


Figure A1. **Fast 3D editing.** Our training method achieves fast 3D editing due to the use of single reference image.

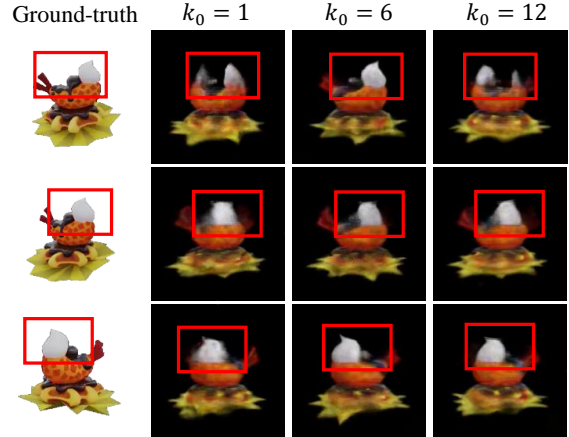


Figure A2. **Ablation study.** Qualitative comparison with various initial k values.

B.2. Potential Applications.

3D editing. Our pose-free training strategy can also be applied to edit a 3D object by propagating edits from a 2D reference view. As illustrated in Figure A1, given a reconstructed 3D object represented by a tri-plane, we can initially edit one reference frame using readily available text-to-image tools based on the user’s prompt. Subsequently, we refine the initial 3D representation by employing our pose-free training strategy, specifically, the training objective detailed in Equation (12) of the main paper.

B.3. Additional Ablation Experiments

Hyper-parameters for Iterative Augmentation. During pose-free training, we first synthesize k pseudo-images and iteratively augment the pseudo-dataset. The initial value of k , denoted as k_0 here, is a crucial hyper-parameter, where higher k_0 results in view inconsistency due to the nature of Zero123-XL [17] (also shown in Fig. 7), and lower k_0 leads to weaker supervision. As an ablation study, we compare the results using different k_0 in Fig. A2. Based on our empirical experience, we recommend a k_0 value between 3 and 8.